

# The Effect of High Magnetic Field on Phase Stability in Fe-Ni

D. M. C. Nicholson<sup>1</sup>, R. A. Kisner<sup>1</sup>, G. M. Ludtka<sup>1</sup>, C. J. Sparks<sup>1</sup>, L. Petit<sup>1</sup>,  
Roger Jaramillo<sup>1</sup>, G. Mackiewicz-Ludtka<sup>1</sup> and J. B. Wilgen<sup>1</sup>, Askar Sheikh-Ali<sup>2</sup>,  
and P. N. Kalu<sup>2</sup>

<sup>1</sup>Oak Ridge National Laboratory  
<sup>2</sup>Florida State University

## Abstract

Identically prepared samples of Fe<sub>0.85</sub>Ni<sub>0.15</sub> were annealed either in the ambient magnetic field or in a field of 29 Tesla. Room temperature X-ray powder diffraction measurements performed after magnetic annealing showed that the ratio of the volume of  $\gamma$  phase to  $\alpha$  phase is decreased in the field annealed sample by a factor of two. First principles calculations of the magnetic structure in the presence of a magnetic field are used to compute the resulting change in free energy. Analysis in terms of the phase diagram calculated with and without a magnetic field is in substantial agreement with measurements.

## Introduction

Phase diagrams typically map the equilibrium phase as a function of temperature, composition, and pressure or another set of equivalent thermodynamic variables. In this paper we emphasize that applied magnetic field should be added to the list of thermodynamic variables, and we give an example where application of a magnetic field leads to a new temperature composition path. Previous work on the application of high fields to Ni-Fe is reviewed by Kakeshita (1). Also, small fields have been used to anneal soft magnetic materials to produce subtle modifications of the local atomic environment that can increase the permeability (2). It is easy to understand why the effect of magnetic fields on phase formation has been little studied. Laboratory fields are typically less than one Tesla and cannot significantly affect the free energy. A simple perturbative estimate of the energy change due to the interaction of the atomic moments with the field,  $\mathbf{m} \cdot \mathbf{B}$ , indicates that a one Tesla field changes the free energy per atom in Fe by about the same amount as changing the temperature by 1 degree. By the same token, applying the highest available fields, 30-40 Tesla is expected to have impacts similar to temperature changes of 30-40 Kelvin; in fact, there is evidence that this underestimates the effects by as much as a factor of two.

There are several ways that magnetic fields can influence microstructure. Most directly, it can change the relative stability of phases at zero temperature. Consider a two phase mixture with different saturation magnetizations. The magnetic induction,  $\mathbf{B}$ , will favor the high magnetization phase by an amount  $(\mathbf{m}_{\text{high}} - \mathbf{m}_{\text{low}}) \cdot \mathbf{B}$ , where  $\mathbf{m}$  is the atomic moment. At finite temperatures there can be additional mechanisms; thermally occupied extended excitations such as spin waves and phonons, and localized excitations such as vacancy facilitated diffusion will be affected. Nucleation will be impacted by field related modification of nucleation barriers and surface energies. Martensite starting temperatures

will be raised. The presence of strong fields will reduce magnetic fluctuations and, hence, magnetic entropy. In ferromagnets the Curie temperature (appropriately defined) will be increased.

Fe alloys are a natural place to look for field induced modifications of phase equilibrium because Fe atoms have large local moments that have strong exchange interactions with their neighbors. Local Fe moments survive to high temperatures and to large percentages of alloy additions (3,4). Furthermore, the directional ordering of Fe moments can vary from ferromagnetic to antiferromagnetic depending on the atomic volume (5). We chose to look at Fe-Ni alloys at compositions in the two phase region between the bcc and fcc solid solutions ( $\alpha$  and  $\gamma$  phases). The temperature was chosen to be 500° C, a temperature at which diffusion is expected to be high enough to allow equilibrium to be approached within a few hours. The selected composition was Fe<sub>85</sub>Ni<sub>15</sub> which lies on the “T<sub>0</sub>” line along which the free energies of  $\alpha$  and  $\gamma$  phases are equal (6). This is also near the Martensite start temperature (7). Placing the alloy at this balance point maximizes the local driving force toward phase separation (see Fig. 1). The transformation can proceed either martensitically i.e. without diffusion, by diffusive decomposition or by a combination. This choice was made to insure that no unforeseen impact of **B** on diffusion obscured the field’s effect on phase stability. The sample should phase separate even without diffusion into bcc and fcc solid solutions. As time passes phase fractions will proceed toward the value prescribed by the lever rule applied to the phase diagram (8) as shown in Fig. 1. We anticipated that application of a large magnetic field would tip the balance in favor of the ferromagnetic bcc phase at the expense of the paramagnetic fcc phase.

### **Procedure**

An alloy of atomic composition Fe<sub>0.85</sub>Ni<sub>0.15</sub> prepared from Ni and Fe stock of 0.999 purity was arc melted in vacuum 5 times and then drop cast into a 10 mm diameter chilled Cu mold in vacuum. The alloy was then homogenized in vacuum for 100 hours at 1100° C. A small amount was ground into powder; the remainder was cut into 10 mm long segments. The powder was made by diamond wheel grinding and was encapsulated in 10 mm diameter stainless steel tubes that were crimped and sealed by electron discharge machining. The crimped tubes were 10 mm long. All powder capsules and cylinders were annealed together at 700° C for 2 hours to obtain the equilibrium  $\gamma$  phase and then were quenched in ice salt brine. The bulk cylinders were electro-polished. A 10 mm rod and a powder sample were subjected to a 29 T field for 245 minutes at 502° C. As a control, one of the identically prepared rods and powder samples was annealed for 245 minutes at 502° C in the ambient field. The samples were rapidly heated from room temperature to 502° C. They were air cooled at a rate of approximately 100° C/min. The field annealed sample remained in the field until it had cooled to a temperature of 85° C at which time the field was turned off.

### **Results**

The volume fractions of the  $\alpha$  and  $\gamma$  phases were determined using Cu K $\alpha$  radiation from a Philips diffractometer with a  $\theta$ -compensating slit. Several diamond peaks resulting from diamond wheel grinding were seen. The diamond peaks are sufficiently separated

from the Fe-Ni peaks that they do not interfere with measurements of the integrated intensities of the Bragg peaks.

In the kinematic approximation to diffraction and with the use of a compensating slit, the integrated intensity associated with a particular reflection hkl is related to the volume fraction  $V_i$  of phase i and the scattering angle  $2\theta$  by (9):

$$P_{hkl,i} = \frac{I_0}{16\pi R} \frac{e^4 V_i m_{hkl} F_i^2}{m^2 c^4 \Omega_i^2} \left( \frac{1 + \cos^2(2\theta)}{2 \sin^2(\theta)} \right) E \left( \frac{\sin(\theta)}{\lambda} \right) \quad (0.1)$$

Here E represents absorption effects not present in an infinitely thick powder in the kinematic limit,  $I_0$  is the beam intensity,  $m_{hkl}$  is the reflection multiplicity,  $R$  is the distance to the detector,  $\lambda$  is the wavelength (1.54 Å),  $\Omega_i$  is the atomic volume, and  $F_i$  is the average atomic scattering factor for the phase i. The scattering factor,  $F_i$  is equal to  $\left| c_i F_{Fe} \left( \frac{\sin(\theta)}{\lambda} \right) + (1 - c_i) F_{Ni} \left( \frac{\sin(\theta)}{\lambda} \right) \right|$  where  $c_i$  is the Fe concentration of phase i and  $F_j$  is the atomic scattering factor of element j. Because Fe and Ni have similar atomic numbers their scattering factors are similar and the average scattering factor at a given  $\theta$  varies by less than 10% for any concentration that can possibly occur in our samples. A further simplifying coincidence is that the scattering factor is independent of concentration near the first  $\alpha$  and  $\gamma$  peaks,  $\sin(\theta)/\lambda = 0.24$ . Therefore, when the ratio of the first two peak intensities is taken, many of the factors in Eqn. 1 cancel and some factors almost cancel. For example, the atomic volumes, scattering amplitudes, and  $\sin(\theta)/\lambda$  are almost equal. Performing these nearly exact cancellations, an extremely simple expression relating  $P_{111\gamma}/P_{110\alpha}$  to the volume ratio is obtained:

$$\frac{m_{110}}{m_{111}} \frac{P_{111\gamma}}{P_{110\alpha}} = \frac{V_\gamma}{V_\alpha} = R_0 \quad (0.2).$$

This simple relation gives the volume fraction  $F_{B=0} = V_{\gamma B=0} / V_{B=0 \text{ total}} = R_{B=0} / (1 + R_{B=0})$  to within one percent of the full expression, Eqn. (1.1).

The integrated intensities under each peak divided by the multiplicity are given in Table 1 along with the value of  $\sin(\theta)/\lambda$  and the atomic scattering factors. The integrated intensities are in arbitrary units and have been normalized to give  $P_{110}/m_{110} = 1.0$  for both samples.

Table 1. Peak intensities divided by peak multiplicity for the  $\alpha$  peaks for anneal with (B=29 T) and without field (B=0 T).

$\alpha$ hkl	110	200	211
P/m B=0	1.000	.468	.256
P/m B=29	1.000	.419	.268
F <sup>2</sup>	313.	267.	178.
$\sin(\theta)/\lambda$	.25	.35	.43

Table 2. Same as Table 1, but for  $\gamma$  peaks.

$\gamma$ hkl	111	200	220	311	222
P/m B=0	.383	.302	.111	.075	.066
P/m B=29	.207	.135	.067	.041	.041
F <sup>2</sup>	312.	254.	172.	133.	122.
sin( $\theta$ ) / $\lambda$	.24	.28	.39	.43	.46

The simplicity of Eqn. 1.2 allows us to read  $R_{B=0}$  from the data for the 110 and 111 peaks; we find  $R_{B=0}=.383$  and  $F_{B=0}=0.28$ . The value 0.28 is smaller than the equilibrium values of  $0.355\pm 0.03$  from application of the lever rule to the phase diagram (8). To put this discrepancy into perspective, consider that an uncertainty in our anneal temperature of  $10^\circ$  C results in an additional uncertainty in the expected volume fraction of  $\pm 0.01$ ; an uncertainty of 1 percent in our alloy composition results in an additional uncertainty in the expected volume fraction of  $\pm 0.03$ . Our uncertainty in temperature and composition should be smaller than  $10^\circ$  C and 1 percent, so our low observed  $\gamma$  volume fraction needs explanation. The difference between our value and the measured equilibrium phase diagram could reflect either that our system has not reached equilibrium or that the value of  $E$  in Eqn. 1.1 is not the same for the two phases. By using data from all peaks we can approximately account for the combined effects of thermal diffuse scattering, surface roughness, finite sample thickness, preferred orientation, and deviations from the kinematic approximation (extinction). Such an analysis gives an average value of  $F_{B=0}=0.30\pm 0.03$  that is consistent with the value 0.28 obtained from the simple formula (1.1) and compares reasonably to the previously measured value of  $0.355\pm 0.03$  from the data of Fig. 1 (8).

This result gives a baseline from which to measure the effect of the magnetic anneal. If we know the relative reduction,  $S=R_{B=0} / R_{B=29}$ , in  $R$  induced by the field we can determine the resulting phase fraction,

$$F_{B=29} = \frac{F_{B=0}}{S + SF_{B=0} - F_{B=0}} \quad (0.3).$$

The value of  $S$  can be deduced from another set of intensity ratios:

$$\frac{\left[ \frac{P_{hkl}^\gamma}{P_{h'k'l'}^\alpha} \right]_{B=0T}}{\left[ \frac{P_{hkl}^\gamma}{P_{h'k'l'}^\alpha} \right]_{B=29T}} = S \frac{\left[ \frac{F^2(c_\gamma, \theta_{hkl}) E_\gamma(\theta_{hkl})}{F^2(c_\alpha, \theta_{h'k'l'}) E_\alpha(\theta_{h'k'l'})} \right]_{B=0T}}{\left[ \frac{F^2(c_\gamma, \theta_{hkl}) E_\gamma(\theta_{hkl})}{F^2(c_\alpha, \theta_{h'k'l'}) E_\alpha(\theta_{h'k'l'})} \right]_{B=29T}} \quad (0.4)$$

provided we have an independent determination of the atomic scattering factor ratios and  $E$  ratios. For the concentration range we are working with, it can be safely assumed that the scattering factor ratios cancel. We find solid evidence that  $E$  is independent of the field. Therefore the ratios involving  $E$  reduce to 1 leaving a very simple expression for  $S$ .

Table 3 gives  $S$  as determined from different  $hkl/h'k'l'$  pairs. Averaging all the data, we obtain  $1.8 \pm 0.2$ . The variability of  $S$  with respect to peak pairs is independent of the atomic scattering amplitude ratio but could reflect changes in  $E$  due to the field. However, the most likely source of error is the background subtraction which was done by visual interpolation of the intensity between Bragg peaks. The 222 peak has the fewest counts and is therefore most sensitive to the determination of the background level; this may account for its uniformly lower value of  $S$ .

Table 3.  $S$  calculated from ratios of peak areas for different peak pairs, (area bcc)/(area fcc).

$\alpha \setminus \gamma$	111	200	220	311	222
100	1.85	2.24	1.67	1.80	1.59
200	1.65	2.00	1.49	1.60	1.42
211	1.94	2.35	1.75	1.88	1.66

Now that  $S$  has been determined we can use Eqn. 1.4, by inserting the volume fraction for the sample annealed in ambient field,  $F_{B=0} = 0.30 \pm 0.03$ , to obtain the  $\gamma$  phase fraction of the field annealed sample. We obtain  $F_{B=29} = 0.14 \pm 0.03$ . This demonstrates that the field reduces the amount of  $\gamma$  phase by a factor of two. The same relative reduction is obtained if the value of  $F_{B=0}$  from the measured phase diagram is used in Eqn. 1.1; the only difference being that the reduction is from 0.36 to 0.16.

## Modeling

For a collinear ferromagnetic material an applied field shifts the Kohn-Sham potential of the majority electrons to lower energy. This shift results in a slight increase of the saturation magnetic moment. As the temperature is increased ferromagnetic materials become slightly non-collinear due thermal excitation of spin waves. Above the Curie temperature the directions of the local moments have no long range correlation and become increasingly random at higher temperatures. The locally self-consistent multiple scattering code (10) was used to calculate the change in energy due to the application of a 30 Tesla field. The additional applied magnetic field contributes a shift in the local Kohn-Sham potential along the direction of the magnetic moment and a rotation of the moment toward the direction of the applied field.

The thermodynamic model of Cheng et al. (6) based on experimental data reproduces the phase diagrams in zero field. We calculate the change in the energy resulting from application of a magnetic field and add this contribution to the existing thermodynamic model. In this way, contributions, which we expect will not be greatly influenced by the magnetic field, such as phonon energy and entropy, can be taken from the existing model. Because we are interested in a temperature well away from the critical temperature we can approximate the change in the partition function by summing over a small number of spin configurations. This procedure fails as the temperature approaches the Curie temperature. Fig. 2 shows the calculated modified free energy curves for Fe-Ni at 500°C. The  $\alpha$  phase is found to have increased stability due to the field of 30 Tesla. The concentration at which the  $\alpha$  and  $\gamma$  curves cross is shifted to higher Ni concentration

indicating an increase in the martensite starting temperature. The field induced change in volume fraction of  $\alpha$  and  $\gamma$  is in qualitative agreement with our measurements.

### **Conclusion**

Because  $S$  can be related so directly to the integrated intensities utilizing a small number of well justified approximations we are confident of the validity of this relative measure of the impact of the magnetic field on the phase ratio. The evaluation of the individual phase fractions requires additional assumptions regarding  $E$ . We are encouraged by the reasonable agreement of our  $B=0$  result with the previously measured phase diagram but have no way of determining whether the small discrepancy results from insufficient equilibration time or dependence of  $E$  on phase. Planned metallography on the bulk cylinders may shed additional light on the initial and final phase fractions.

### **Acknowledgements**

Research sponsored by the Laboratory Directed Research and Development Program of Oak Ridge National Laboratory (ORNL), managed by UT-Battelle, LLC for the U. S. Department of Energy under Contract No. DE-AC05-00OR22725. Calculations performed at the National Energy Research Computing Center and the Center for Computational Sciences, Oak Ridge National Laboratory.

## References

- <sup>1</sup> Ken'ichi Shimizu and Tomoyuki Kakeshita, *ISIJ International*, **29**, 97 (1989).
- <sup>2</sup> Bozorth, *Ferromagnetism*, D Van Nostrand Co. New York (1951). John C. Slonczewski, in *Magnetic Ions in Insulators Their Interactions, Resonances, and Optical Properties*. Editor George T. Rado, Academic Press, New York (1963).
- <sup>3</sup> Y. Waseda and K Suzuki, *Phys Stat Solidi* **39**, 669 (1970).
- <sup>4</sup> T Hoshino, R. Zeller, and P. H. Dederichs, *J. Mag. Mag. Mat.* 140, 113 (1995).
- <sup>5</sup> M. Uhl et al., *Phys. Rev. B* **50**, 291 (1994).
- <sup>6</sup> Ying-Yu Chuang, Y. Austin Chang, Rainer Schmid, and Jen-Chewn Lin, *Metall. Mater. Trans.* **17A**, 1361 (1986).
- <sup>7</sup> Y. E. A Fokina, L. V. Smirnov, V. D. Sadovsky, *Fiz. Metal. Metalloved.*, 27, 756 (1969).
- <sup>8</sup> J. Zhang, D. B. Williams, and J. I. Goldstein, *Metall. Mater. Trans.* **25A**, 1639 (1994).
- <sup>9</sup> B. E. Warren *X-Ray Diffraction*, Dover Publications, New York (1969)
- <sup>10</sup> Y. Wang, G.M. Stocks, W.A. Shelton, D.M.C. Nicholson, W.M. Temmerman, and Z. Szotek, *Phys. Rev. Lett.* **75**, 2867 (1995).

Figure 1. Fe rich section of phase diagram showing martensite start-temperature, equal free energy line, and decomposition path at 500° C (8).

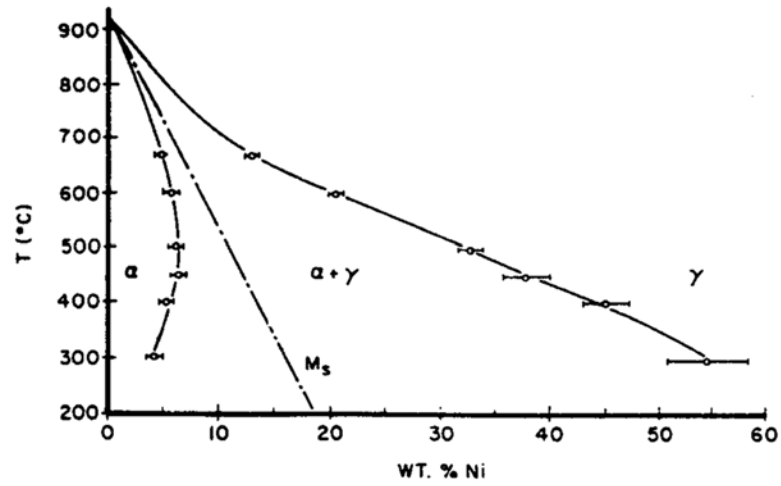


Figure 2. Free energy with and without applied field. Arrows indicate the phase concentrations.

